Vol. 81 No. 3 pp. 463–469 ACTA GEOLOGICA SINICA June 2007

Burial Records of Reactive Iron in Cretaceous Black Shales and Oceanic Red Beds from South Tibet

Huang Yongjian[1, *], Wang Chengshan[1], Hu Xiumian[2] and Chen Xi[1]
1 *Research Center for Tibetan Plateau Geology, China University of Geosciences (Beijing), Beijing 100083*
2 *Department of Earth Sciences, Nanjing University, Nanjing, Jiangsu 210093*

Abstract: One of the new directions in the field of Cretaceous research is to elucidate the mechanism of the sedimentary transition from the Cretaceous black shales to oceanic red beds. A chemical sequential extraction method was applied to these two types of rocks from south Tibet to investigate the burial records of reactive iron. Results indicate that carbonate-associated iron and pyrite are relatively enriched in the black shales, but depleted or absent in red beds. The main feature of the reactive iron in the red beds is relative enrichment of iron oxides (largely hematite), which occurred during syn-depostion or early diagenesis. The ratio between iron oxides and the total iron indicates an oxygen-enriched environment for red bed deposition. A comparison between the reactive iron burial records and proxies of paleo-productivity suggests that paleo-productivity decreases when the ratio between iron oxides and the total iron increases in the red beds. This phenomenon could imply that the relationship between marine redox and productivity might be one of the reasons for the sedimentary transition from Cretaceous black shale to oceanic red bed deposition.

Keywords: reactive iron, black shales, oceanic red beds, Cretaceous, south Tibet

1 Introduction

The Earth System might be in a greenhouse climate state during the whole Cretaceous time. Oceanic anoxic events (OAEs) have long been one of the important subjects of Cretaceous paleo-oceanography (e.g. Schlanger and Jenkyns, 1976; Jenkyns, 1980). It has been suggested that oceanic bottom water may have been dysoxic to anoxic at this time, which led to wide distribution of organic-carbon enriched black shales in a deep oceanic basin (Leckie et al., 2002). However, it has been found, especially after the implementation of the two international geosciences programs (IGCP 463/494), that hemi-pelagic to pelagic red sediments (Cretaceous oceanic red beds, CORB; Wang et al., 2004; Hu et al., 2005) are the main type of deposit when black shale deposition ended, implying that the deep ocean would have gone quickly to an oxic state after the OAEs (Wang et al., 2005). The transition from black shales to red sediments is related to important problems such as the global change and carbon-oxygen cycle under greenhouse climate, and has become a new and important focus of Cretaceous research (Wang and Hu, 2005).

Black shales and red beds are well-preserved in south Tibet (Wang et al., 2001), and have previously been investigated in terms of stratigraphy (Wang et al., 2000; Li et al., 2005), paleontology (Wan et al., 2005), sedimentology and lithology (Hu et al., 2006), and geochemistry (Wang et al., 2005, Zou et al., 2005). The present study is focused on the development of burial records for reactive iron (see later definition) during the black shale to red bed transition, and will explore the paleo-oceanographical significance of these records, so as to carry the work a step forward.

2 Geological Setting

Located in Gyangzê County, Tibetan, the studied region (Fig. 1) is tectonically part of the northern subzone of the Tethyan Himalayas (Yu and Wang, 1990). Cretaceous sediments in this area deposited in a slope-basin environment, which outcrops most completely in the Chuangde section (Fig. 1). Wang et al. (2000) redefined the stratigraphy along the section; and Chen (2005)

* Corresponding author. E-mail: huangyj@cugb.edu.cn.

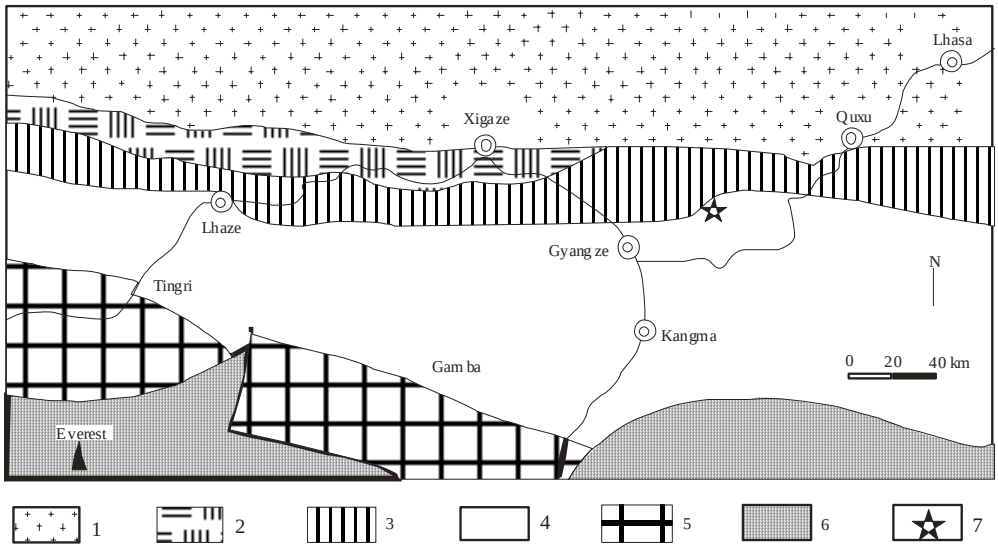

Fig. 1. Geological setting of study region and locality of the Chuangde section.
1. Gandgdise magmatic arc; 2. Xigazê forearc basin; 3. Yarlung Zangbo suture zone; 4. northern subzone of the Tethyan Himalayas; 5. southern subzone of the Tethyan Himalayas; 6. crystal Himalayan zone; 7. position of Chuangde section.

measured the section again in more detail. The Cretaceous strata, 210 m thick in total, can be divided into the Gyabula, Chuangde and Zongzuo Formations. Aged from Barriacian to early Santonian, the Gyabula Formation consists of two segments: (1) a black unit from 0 to 63 m, which is mainly black shale with almost no carbonate and aged from Barriacian to Albian; (2) a white unit from 63 to 169 m thick and aged from Cenomanian to early Santonian, which is composed of grey to black siliceous or calcareous shales with a much higher carbonate content. Pyrite nodules can be found within this unit and the white colouration is because of weathering. The Chuangde Formation consists mainly of red shales intercalated with red marls and red carbonates. Planktonic foraminifera and calcareous nannofossils define the age of the Chuangde Formation as the late Santonian to the early Campanian. The Zongzuo Formation is composed predominantly of dark grey to black shale enclosing various olistoliths of sandstone, limestone and bedded chert. This work covered the samples from 68 to 197.6 m in the Chuangde section, including the Gyabula (white unit) and Chuangde Formations. For further details describing the section see Chen (2005).

3 Definition of Reactive Iron, Methods and Samples

As one of the most abundant redox sensitive elements in the crust, iron occurs as distinct minerals according to the redox condition during syn-deposition and early diagenesis (Chen and Wang, 2004). If the system is in a more reducing state, detrital iron oxides will likely be reduced (either partly or completely), ultimately forming carbonate-associated iron (including siderite) or pyrite (Canfield, 1989). By contrast, if the system is in an oxygen-enriched state, new iron oxdes will be formed in the sediments (Glasby, 1991). Chemical sequential extraction techniques can be applied to the sediments to estimate the content of carbonate-associated iron (including siderite), pyrite and iron oxides, which can give important information about the redox condition of the depositional environment (Berner, 1970; Raiswell et al., 1988; Canfield, 1989; Raiswell et al., 1994; Raiswell and Canfield, 1998; Raiswell et al., 2001; Poulton and Canfield, 2005). Because these types of iron are the main iron species active at the stage from syn-deposition to early diagenesis, the sum of the iron present in these minerals is commonly referred to as highly reactive iron (Fe_{HR}; Berner, 1970; Canfield, 1989; Raiswell and Canfield, 1998). Related studies have been successful in resolving problems related to the redox evolution of the paleo-ocean (Raiswell et al., 1988; Raiswell et al., 2001; Canfield et al., 2007), and the low-temperature geochemical cycle of iron (Poulton and Raiswell, 2002).

On the basis of previous work, Poulton and Canfield (2005) developed a comprehensive method for marine sediments, which includes carbonate-associated iron (Fe_{carb}), easily reducible iron (ferrihydrite and lepidocrocite, Fe_{ox1}), reducible iron (goethite and hematite, Fe_{ox2}), magnetite (Fe_{mag}), pyrite (Fe_{py}), sheet silicate iron (Fe_{PR}) and unreactive iron (the difference between the total Fe and all other forms of iron, Fe_U). For ancient sediments, the ferrihydrite and lepidocrocite have been transformed into goethite or hematite, the Fe_{ox1} and Fe_{ox2} fractions are often combined via a single extraction to give a total ferric oxide pool (Fe_{ox}).

Fifty samples from the Chuangde section were analyzed using this method (Poulton and Canfield, 2005) in the Geochemical Lab, University of Newcastle Upon Tyne, U.K. The sampling intervals were 4 m for the white unit and 1–2 m for the red beds. Fe_{carb}, Fe_{ox}, Fe_{mag} and Fe_{py} were determined for each sample. Highly reactive iron (Fe_{HR}) was acquired when adding these four forms of iron

together, and the total iron (Fe_T) was determined in Nanjing University. All data are listed in Table 1.

4 Results

The ranges and averages of the different iron pools are summarized in Table 2. In the red beds, Fe_T, Fe_{ox}, Fe_{mag} and Fe_{HR} average 8.69%, 2.62%, 0.59% and 3.25%, respectively, and are relatively higher than those in the black shales. The averages for Fe_T, Fe_{ox}, Fe_{mag} and Fe_{HR} in the latter are 4.25%, 0.38%, 0.13% and 0.64%. However, black shales are relatively enriched in Fe_{carb} and Fe_{py} with averages of 0.13% and 0.007%, respectively. Pyrite was below detection in the red beds and the mean Fe_{carb} content is 0.04%.

Because the absolute content of the different iron fractionations is affected by the total amount of Fe_T, the ratio between iron fractions and total iron is used to more effectively reflect the distribution of different iron fractions and therefore changes in the depositional environment (Poulton and Raiswell, 2002). However, from the normalized results (Table 3), the features of the distribution of iron fractions are essentially the same. The Fe_{ox}/Fe_T, Fe_{mag}/Fe_T, Fe_{HR}/Fe_T ratios are still higher in the red beds, while Fe_{carb}/Fe_T and Fe_{py}/Fe_T are still higher in the black shales (white unit), which indicates that the variations in the total reactive iron (Fe_{HR}) contents and species (Fe_{carb}, Fe_{ox}, Fe_{mag}, Fe_{py}) mainly result from the changes in the depositional environment.

5 Discussion

Previous work has shown that red beds of the Chuangde Formation corresponding to a more-oxic depositional environment than the underlying Gyabula Formation although this was not based on a direct proxy for the oxic depositional environment of red beds (Wang et al., 2005). The mechanism for the occurrence and duration of red beds is also poorly constrained (Wang et al., 2005; Hu et al., 2006). However, the differences between reactive iron burial in the black shales and red beds presented here may give some new insights into these problems.

There is essentially no pyrite and Fe_{carb} (the ferrous iron-bearing phases) in the red beds, which suggests an oxygen-enriched depositional environment relative to the underlying black shales. The much lower Fe_{mag}/Fe_T in the white unit may be due to the anoxic dissolution of magnetite by sulfide during the early diagenesis of these sediments (Canfield and Berner, 1987). Fe_{ox}/Fe_T contributes to more than 80% of the total difference in Fe_{HR}/Fe_T between the black shales and red beds. Fe_{ox}/Fe_T in the red beds is not only higher than that in the white unit, but also higher than that in modern continental margin and deep sea sediments (0.28 and 0.25, respectively), and higher than that in the Jurrasic and Cretaceous non-red oceanic sediments (0.16), but lower than that in the modern oceanic red clay (0.33, Poulton et al., 1998; Poulton and Raiswell, 2002). In these red sediments, Fe_{ox} mainly represents hematite (Hu et al., 2006), and it is concluded that the relatively high Fe_{ox}/Fe_T ratios observed in the red beds is due to the existence of excess hematite. In the study of clay minerals in the Chuangde section (Hu, 2002), it is suggested that the weathering situation in the source region did not change greatly during deposition of the Gyabula and Chuangde Formations. This suggests that the change of Fe_{ox}/Fe_T between the black shales and red beds is not caused by the variation of Fe_{ox}/Fe_T in the detrital input (Poulton and Raiswell, 2002). The increase in Fe_{ox}/Fe_T in the red beds therefore likely occurred during the phase from syn-deposition to early diagenesis, which is also implied by petrological and mineralogical evidence (Hu et al., 2006). Case studies on Cretaceous oceanic red beds from elsewhere also suggest that the enrichment in iron oxides (excess hematite) occurred in the period from syn-deposition to early diagenesis (Channell, 1982; Eren and Kadir, 1999). On the other hand, the enrichment of iron oxides, i.e., the formation of excess hematite, in the Chuangde Formation may indicate that the depositional environment was in an oxygen-enriched state (Hu, 2002; Wang et al., 2005; Hu et al., 2006), and the Fe_{ox}/Fe_T ratio may be an indication of the development of an oxygen-enriched environment for red beds deposition.

Previous investigations have suggested that oceanic paleoproductivity decreased during red bed deposited (Wang et al., 2005; Zou et al., 2005). The main evidence relates to a negative organic carbon isotope excursion (Fig. 2), and a decrease in biogenic barium contents (Ba/Al) (Zou et al., 2005). Coeval negative trends can also be found from inorganic carbon isotope records in a more shallow area of south Tibet (Hu, 2002), which also supports the conclusion of decreased marine productivity and lower burial of organic carbon. Therefore, during the deposition of red sediments, the development of oxygen-enriched conditions was accompanied by a decrease in paleoproductivity, which may imply that a feedback existed between the redox state and productivity of the ocean.

According to observations for the modern ocean, the iron cycle is related to the cycling of several elements, and is especially coupled to that of phosphorus (Anschutz, et al., 1997; Weng, 1999). Under oxygen-enriched conditions, reactive iron species in marine sediments will be buried mostly as iron oxides, and more phosphorus will

Table 1 Analytical results of reactive iron for upper Cretaceous samples from southern Tibet

Sample	Lithology	Fe_T	Fe_{carb}	Fe_{ox}	Fe_{mag}	Fe_{py}	Fe_{HR}
04cd067	Black shale	4.92	0.17	0.32	0.22	0.0014	0.70
04cd072	Black shale	4.48	0.16	0.09	0.20	0.0155	0.47
04cd076	Black shale	5.39	0.12	0.37	0.17	0.0006	0.66
04cd080	Black shale	5.66	0.17	0.68	0.22	0.0114	1.08
04cd084	Black shale	5.14	0.17	0.32	0.22	0.1324	0.84
04cd088	Black shale	4.31	0.20	0.31	0.20	0.0047	0.71
04cd092	Black shale	3.27	0.10	0.36	0.11	0.0007	0.57
04cd096	Black shale	3.39	0.11	0.18	0.10	0.0032	0.39
04cd100	Grey marlstone	5.85	0.15	0.25	0.23	0.0019	0.62
04cd104	Black shale	2.88	0.09	0.25	0.08	0.0019	0.42
04cd108	Black shale	6.20	0.13	0.54	0.20	0.0011	0.88
04cd112	Grey marlstone	2.69	0.12	0.09	0.06	0.0044	0.28
04cd116	Grey marlstone	2.31	0.10	0.23	0.06	0.0040	0.40
04cd120	Grey marlstone	4.08	0.14	0.33	0.15	0.0026	0.63
04cd124	Black shale	3.02	0.10	0.38	0.07	0	0.54
04cd128	Grey marlstone	2.63	0.08	0.34	0.06	0.0005	0.48
04cd132	Black shale	3.14	0.07	0.43	0.08	0.0053	0.58
04cd136	Marlstone	3.26	0.06	0.44	0.07	0	0.57
04cd140	Marlstone	2.78	0.10	0.46	0.07	0.0007	0.63
04cd144	Marlstone	2.89	0.08	0.28	0.05	0.0018	0.42
04cd148	Siliceous rock	3.32	0.12	0.33	0.06	0	0.51
04cd150	Siliceous rock	2.24	0.05	0.24	0.06	0	0.35
04cd154	Siliceous rock	2.88	0.12	0.28	0.02	0.0029	0.42
04cd158	Siliceous rock	4.79	0.09	0.46	0.10	0.0042	0.66
04cd162	Siliceous rock	4.03	0.16	0.55	0.10	0	0.82
04cd166	Siliceous rock	9.24	0.17	0.19	0.05	0	0.41
cd051	Grey shale	7.81	0.14	1.50	0.38	0	2.03
cd052	Red shale	8.48	0.07	2.80	0.64	0	3.51
cd053	Red shale	7.15	0.02	1.68	0.55	0	2.24
cd056	Red shale	10.07	0.01	4.43	0.61s	0	5.05
cd063	Red shale	9.93	0.03	3.08	0.63	0	3.74
cd071	Red shale	8.50	0.01	2.49	0.57	0	3.07
cd077	Red shale	8.40	0.02	2.92	0.63	0	3.57
cd083	Red marlstone	1.38	0.01	0.50	0.09	0	0.60
cd086	Red shale	5.03	0.02	1.54	0.38	0	1.94
cd092	Red shale	11.38	0.06	4.14	0.75	0	4.95
cd100	Violet siliceous shale	11.43	0.03	4.14	0.84	0	5.02
cd105	Red shale	11.61	0.02	3.66	0.81	0	4.49
cd113	Violet siliceous shale	11.87	0.03	3.66	0.85	0	4.55
cd133	Violet siliceous shale	11.93	0.01	3.61	0.81	0	4.42
cd35w1	Red marlstone	2.00	0.02	0.50	0.12	0	0.64
cd142	Violet calcareous shale	11.53	0.02	4.07	0.90	0	4.99
cd35w2	Red marlstone	5.11	0.04	1.25	0.29	0	1.58
cd158	Red shale	12.66	0.06	3.34	0.84	0	4.24
cd35w3	Red marlstone	5.90	0.07	1.19	0.39	0	1.65
cd166	Red shale	10.13	0.05	2.30	0.66	0	3.01
cd174	Red shale	10.61	0.04	2.86	0.65	0	3.54
cd36w2	Red marlstone	7.17	0.05	1.76	0.58	0	2.38
cd36w3	Red marlstone	6.24	0.11	1.54	0.38	0	2.03
cd187	Red shale	11.23	0.01	2.81	0.60	0	3.42
cd190	Green-grey calcareous shale	6.27	0.22	0.94	0.17	0	1.33

Note: the content is in percent (%). Fe_{carb}, Fe_{ox}, Fe_{mag} and Fe_{py} are carbonate-associated iron, ferric iron oxides (mainly goethite and hematite), magnetite and pyrite, respectively. Fe_{HR} is the total content of reactive iron species. Fe_T is the total amount of iron in the sample.

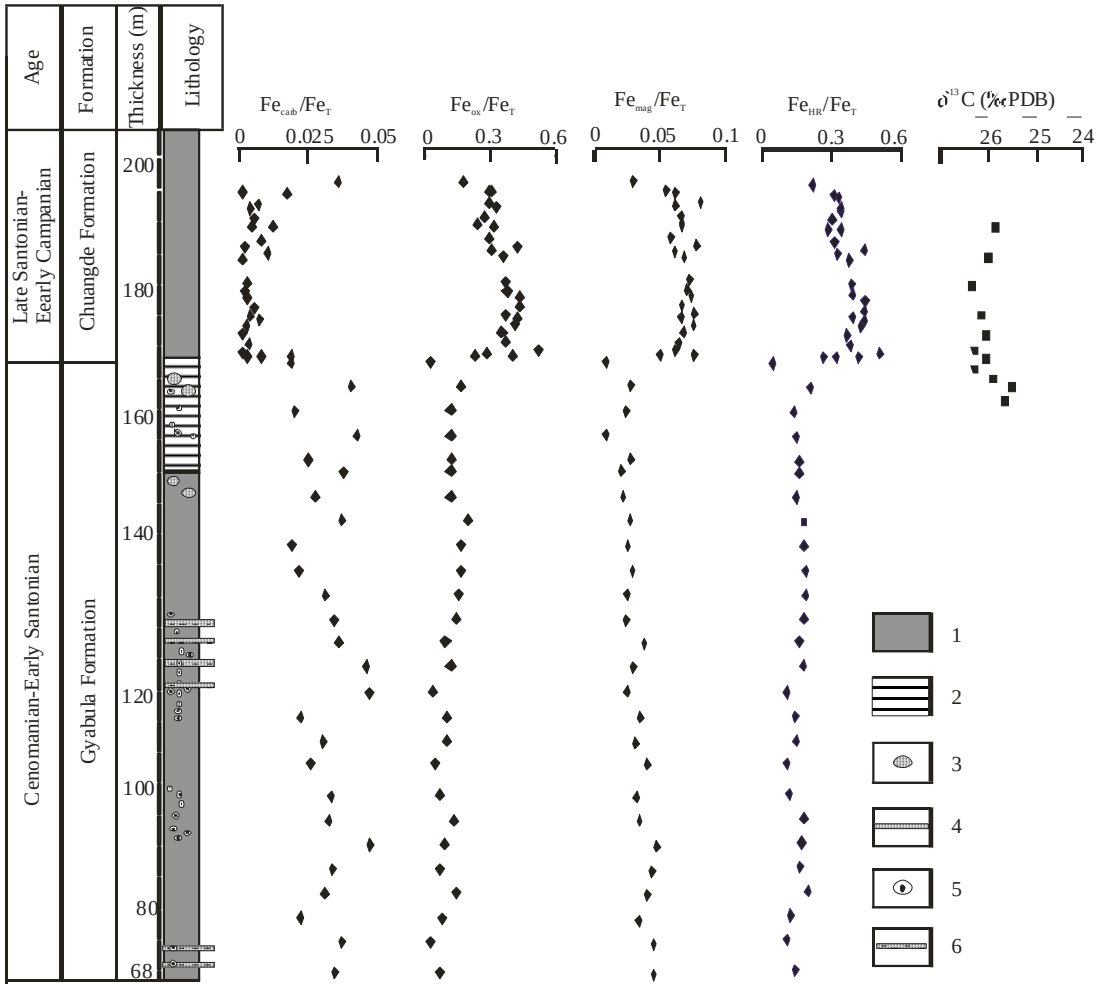

Fig. 2. Part of reactive iron burial records and organic carbon isotope curve from the Chuangde section, south Tibet (Organic carbon isotope data is from Zou et al., 2005).
1. Shale; 2. siliceous rock; 3. pillow-like limestone; 4. limestone; 5.nodule; 6. bedded limestone.

be absorbed onto iron oxides and therefore buried (Slomp et al., 1996), resulting in less phosphorus regeneration to the overlying sea water (Colman and Holland, 2000). This leads to a decrease in phosphorus cycling efficiency in the ocean, relative to anoxic conditions. Phosphorus is the ultimate limiting nutrient for marine production on geological timescales, and the decrease in phosphorus cycling efficiency would lead to a less productive ocean (Tyrrell, 1999). Such a feedback mechanism between the redox state and productivity of the ocean (VanCappellen and Ingall, 1996; Berner et al., 2003) would help to maintain oxygen-enriched conditions in the deep ocean, and would therefore be favorable for the continued deposition of red beds. The negative relation between Fe_{ox}/Fe_T and paleoproductivity, and the relative enrichment of phosphorus in the red beds of the Chuangde Formation (Hu, 2002) suggest that this feedback mechanism may be a reason for the transition from Cretaceous black shales to oceanic red beds deposition, while other factors such as climate and ocean circulation would also have played important roles (Wang et al., 2005).

Table 2 Summarization of iron speciation and FeT in the white and red unit of the Chuangde section

	Fe_{carb}		Fe_{ox}		Fe_{mag}		Fe_{py}		Fe_{HR}		Fe_T	
	Range	Average	Range	Average	Range	Average	Range	Average	Range	Average	Range	Average
White unit	0.07 −0.22	0.13	0.09 −1.50	0.38	0.02− 0.38	0.13	0.0 −0.1324	0.007	0.28 −2.03	0.64	2.24 −9.24	4.25
Red unit	0.01 −0.11	0.04	0.50 −4.14	2.62	0.09 −0.90	0.59	0.0	0.0	0.60 −5.05	3.25	1.38 −12.7	8.69

Note: the content is in percent (%). The averages are calculated as numerical means.

Table 3 Summarization of the ratio between reactive iron species and total iron in white and red unit of the Chuangde section

	Fe_{carb}/Fe_T		Fe_{ox}/Fe_T		Fe_{mag}/Fe_T		Fe_{py}/Fe_T		Fe_{HR}/Fe_T	
	Range	Average	Range	Average	Range	Average	Range	Average	Range	Average
White unit	0.018 –0.047	0.031	0.02 –0.19	0.10	0.005 –0.05	0.028	0.0 –0.025	0.0015	0.04 –0.26	0.161
Red unit	0.008 –0.0169	0.006	0.201 –0.439	0.296	0.05 –0.08	0.067	0	0	0.28 –0.50	0.37

6 Conclusions

The following conclusions can be made according to the above discussion and interpretations on the reactive iron data of Cretaceous black shale and oceanic red beds:

(1) No pyrite can be found and carbonate-associated iron is much lower in the red beds. The main characteristic of reactive iron in the red beds is the enrichment of iron oxides (largely hematite).

(2) The enrichment of iron oxides occurred during the stage from syn-depostion to early diagenesis. The ratio between hematite to the total iron (Fe_{ox}/Fe_T) can indicate an oxygen-enriched depositional environment for red beds.

(3) A correlation has been done between the reactive iron burial records and proxies of paleo-productivity, which suggests that paleo-productivity decreases when the ratio between iron oxides and the total iron (Fe_{ox}/Fe_T) increases in the red beds. This phenomenon could imply that the feedback between marine redox condition and productivity (i.e., the oxygen-enriched ocean corresponding to lower productivity), might be one of the reasons for the sedimentary transition from Cretaceous black shales to oceanic red beds.

Acknowledgements

Advices were given by Prof. Wolfgang Kuhnt from Kiel University, Germany and Prof. Li Xianghui from Chengdu University of Technology, China, during the fieldwork. The authors are in debt to Prof. Rob Raiswell from University of Leeds, U.K., and many colleagues from IGCP 463/494 for their helpful discussions during the preparation of the manuscript. This work is supported by the National Key Basic Research Program (2006CB701406), Natural Science Foundation of China for Youth (40403003) and Key Project of the Natural Science Foundation of China (40332020), and is a contribution to IGCP 463.

Manuscript received March 5, 2007
accepted May 15, 2007
edited by Susan Turner

References

Anschutz, P., Zhong, S.J., and Sundby, B., 1998. Burial efficiency of phosphorus and the geochemistry of iron in continental marine sediment. *Limnology and Oceanography*, 43(1): 53–64.

Berner, R,A., Beerling, D.J., and Dudley. R., 2003. Phanerozoic atmospheric oxygen. *Annual Rev. Earth Planet. Sci.*, 31: 105–134.

Berner, R.A., 1970. Sedimentary pyrite formation. *Am. J. Sci.*, 268: 1–23.

Canfield, D.E., 1989. Reactive iron in marine sediments. *Geochim. Cosmochim. Acta*, 53: 619–632.

Canfield, D.E., and Berner, R.A., 1987. Dissolution and pyritization of magnetite in anoxic marine sediments. *Geochim. Cosmochim. Acta*, 51: 645–659.

Canfield, D.E., Poulton, W.S., and Narbonne, G.M., 2007. Late-Neoproterozoic Deep-Ocean oxygenation and the rise of animal life. *Science*, 315: 92–95.

Channell, J.E., Freeman, R., and Heller, F., 1982. Timing of diagenetic hematite growth in red pelagic limestones from Gubbio (Italy). *Earth Planet. Sci. Lett.*, 58: 189–201.

Chen Jun and Wang Helian, 2004. *Geochemistry*. Beijing: Scientific Publishing House, 418 (in Chinese).

Chen Xi, 2005. Chemostratigraphy in marine Cretaceous of Gyangzê area, Southern Tibet. Master Thesis. Chengdu: Chengdu University of Technology, 70 (in Chinese with English Abstracts).

Colman, A.S., and Holland, H.D., 2000. The global diagenetic flux of phosphorus from marine sediments to the oceans: redox sensitivity and the control of atmospheric oxygen levels. In: Glenn, C.R. (ed.), *Marine Authigenesis: From Global to Microbial*: Society of Sedimentary Geological Special Publication, 66: 53–75.

Leckie, R.M., Bralower, T.J., and Cashman, R., 2002. Oceanic anoxic events and plankton evolution: Biotic response to tectonic forcing during the mid-Cretaceous. *Paleoceanography*, 17: 623–642.

Eren, M., and Kadir, S., 1999. Color origin of Upper Cretaceous pelagic red sediments within the Eastern Pontides, northeast Turkey. *Intl. J. Earth Sci.*, 88: 593–595.

Glasby, G.P., 1991, Mineralogy, geochemistry, and origin of Pacific red clays: a review. *New Zealand J. Geol. Geophys.*, 34: 167–176.

Hu Xiumian, 2002. Cretaceous sedimentary geology in southern Tibet and upper Cretaceous oceanic red beds-the oxic event. Ph.D Thesis. Chengdu: Chengdu University of Technology, 216 (in Chinese with English Abstracts).

Hu Xiumian, Wang Chengshan and Li Xianghui, 2006. Upper Cretaceous oceanic red beds in southern Tibet: petrology, sedimentary environments, and colour origin. *Sci. China* (D), 36: 811–821.

Hu, X.M., Jansa, L., and Wang, C.S., 2005. Upper Cretaceous Oceanic Red beds (CORB) in the Tethys: Occurrence, lithofacies, age and environment. *Cretaceous Res.*, 26: 3–18.

Jenkyns, H.C., 1980. Cretaceous anoxic events: from continents to oceans. *J. Geol. Soc. London*, 137: 171–188.

Li, X.H., Wang, C.S., and Hu, X.M., 2005. Stratigraphy of deep-water Cretaceous deposits in Gyangzê, southern Tibet, China. *Cretaceous Res.*, 26: 33–41.

Poulton, W.S., Bottrell, S.H., and Underwood, C.J., 1998, Pore-water sulfur geochemistry and fossil preservation during phosphate diagenesis in a Lower Cretaceous shelf mudstone. *Sedimentology*, 45: 875–887.

Poulton, W.S., and Canfield, D.E., 2005. Development of a sequential extraction procedure for iron: implications for iron partitioning in continentally derived particulates. *Chemical Geol.*, 214: 209–221.

Poulton, W.S., and Raiswell, R., 2002. The low-temperature geochemical cycle of iron: from continental fluxes to marine sediment deposition. *Am. J. Sci.*, 302: 774–805.

Raiswell, R., Buckley, F., and Berner, R.A., 1988. Degree of pyritization of iron as a paleoenvironmental indicator of bottom-water oxygenation. *J. Sediment. Petrol.*, 58: 812–819.

Raiswell, R., and Canfield, D.E., 1998. Sources of iron for pyrite formation in marine sediments. *Am. J. Sci.*, 298: 219–245.

Raiswell, R., Canfield, D.E., and Berner, R.A., 1994. A comparison of iron extraction methods for the determination of degree of pyritization and the recognition of iron-limited pyrite formation. *Chemical Geol.*, 111: 101–110.

Raiswell, R., Newton, R., and Wignall, P.B., 2001. An indicator of water-column anoxia: resolution of biofacies variations in the reduced inorganic sulfur in sediments and shales. *Chemical Geol.*, 54: 149–155.

Schlanger, S.O., and Jenkyns H.C., 1976. Cretaceous oceanic anoxic events: cause and consequence. *Geologie en Mijnbown*, 55: 179–184.

Skelton, P.W., 2003. *The Cretaceous World*. London: Cambridge University Press, 350.

Slomp, C.P., Van der Gaast, S.J., and Van Raaphorst, W., 1996. Phosphorus binding by poorly crystalline iron oxides in North Sea sediments. *Marine Chem.*, 52: 55–73.

Tyrrell, T., 1999. The relative influences of nitrogen and phosphorus on oceanic primary production. *Nature*, 400: 525–531.

Van Cappellen, P., and Ingall, E.D., 1996. Redox stabilization of the atmosphere and oceans by phosphorus-limited marine productivity. *Science*, 271: 493–496.

Wan, X.Q., Lamolda, M.A., and Si, J.L., 2005. Foraminiferal stratigraphy of Late Cretaceous red beds in southern Tibet. *Cretaceous Res.*, 26: 43–48.

Wang Chengshan and Hu Xiumian, 2005. Cretaceous world and oceanic red beds. *Geosciences Frontier*, 12(2): 11–21 (in Chinese with English abstracts).

Wang Chengshan, Li Xianghui, Wan Xiqoqiao and Tao Rao, 2000. The Cretaceous in Gyangzê, Southern Xizang (Tibet): redefined. *Acta Geologica Sinica* (Chinese edition), 74(2): 97–107 (in Chinese with English Abstracts).

Wang, C.S., Hu, X.M., and Jansa, L., 2005. Upper Cretaceous oceanic red beds in southern Tibet: a major change from anoxic to oxic condition. *Cretaceous Res.*, 26: 21–32.

Wang, C.S., Hu, X.M., and Jansa, L., 2001. The Cenomanian-Turonian oceanic anoxic event in southern Tibet. *Cretaceous Res.*, 22: 481–490.

Wang, C.S., Huang, Y.J., and Hu, X.M., 2004. Cretaceous oceanic red beds: Implications for paleoclimatology and paleoceanography. *Acta Geologica Sinica* (English edition), 78: 873–877.

Weng Huanxin, 1999. The significance of sedimentary phosphorus in the continental margin for the study of global change. *Advance Earth Sci.*, 14(5): 524–527 (in Chinese with English Abstracts).

Yu Guangming and Wang Chengshan, 1990. *Sedimentary Geology in Tibetan Tethys*. Beijing: Geological Publishing House, 185 (in Chinese with English Abstracts).

Zou, Y.R., Kong, F., and Peng, P.A., 2005. Organic geochemical characterization of Upper Cretaceous oxic oceanic sediments in Tibet, China: A preliminary study. *Cretaceous Res.*, 26: 65–71.